Ionics
https://doi.org/10.1007/s11581-020-03506-8

ORIGINAL PAPER

Stability study of triple layer hollow fiber in solid oxide fuel cell with methane as fuel

Mohd Hilmi Mohamed[1,2] · Mohd Hafiz Dzarfan Othman[1] · Mohd Zamri Mohd Yusop[2] · Siti Khadijah Hubadillah[1] · Yuji Iwamoto[3] · Suriani Abu Bakar[4] · Hamzah Fansuri[5]

Received: 5 March 2019 / Revised: 29 January 2020 / Accepted: 21 February 2020

Abstract

Solid oxide fuel cell (SOFC) is an attractive device that can convert chemical into energy. Recently, the triple layer hollow fiber (TLHF) opens up a new discovery of higher power output. This study investigates the fabrication of TLHF in solid oxide fuel cell consisting anode/anode functional layer (AFL)/electrolyte (NiO-YSZ/NiO-YSZ/YSZ) via single-step phase inversion-based co-extrusion combined with co-sintering technique using methane as fuel. TLHF formed sandwich-like structure that corresponds to the anode and AFL with dense electrolyte. Initially, the open circuit voltage (OCV) was 1.1 V, after 90 min, the OCV dropped to 0.2 V due to the carbon deposits that caused poisoning. Meanwhile, the power density also reduces from 0.8 to 0.33 Wcm^{-2}. SEM image carbon shows the carbon deposited causing crack and reached electrolyte layer. TEM of the Ni catalyst indicates there are multilayer of graphite exhibit at the Ni particle courtesy of the carbon deposits. The results showed the graphite causing the performance to decrease which is corresponding to the usage of methane as fuel.

Keywords Triple layer hollow fiber · Solid oxide fuel cell · Methane · Stability

Introduction

Solid oxide fuel cell (SOFC) has recently been gaining attention due to its high power density [1], compact design [2], and fuel flexibility [3]. In SOFC, there are currently three (3) geometries that are being extensively being researched which are planar, tubular, and micro-tubular (hollow fiber) [4]. The micro-tubular configuration of SOFC shows promising potential in the future due to several advantages such as producing high power output and compact in size [5]. The reduction of unit size helps to increase in the power density as it is highly related to the tube diameter [4, 6]. In such cases, a single 2 mm diameter micro-tubular SOFC can provide up to 10-fold power per stack volume than a 20-mm counterpart [2, 7]. Another advantage in micro-tubular design is its high thermal shock resistance [8]. While the larger diameter was prone to cracking, the micro-tubular SOFC does not crack even at operating temperature of 850 °C. However, the performance of the hollow fiber hindered by the contact resistance that occurred at between electrolyte and anode. This issue had been addressed in few researchers [9–12]. Due to this, micro-tubular solid oxide fuel cell that consisting of anode, anode functional layer (AFL), and electrolyte was extensively studied.

The application of AFL that sandwiched between electrolyte and anode causes the cell to increase the performance while simultaneously reducing the resistance between the layer [13]. The research by Suzuki et al. [14] shows the performance of the cell with AFL improved from 0.27 to 0.45 Wcm^{-2}. Meanwhile, Chen et al. [15] were able to record cell performance of 2.6 Wcm^{-2} by using Ni-YSZ as the anode and AFL layer. This is also in agreement with the finding by

✉ Mohd Hafiz Dzarfan Othman
dzarfan@utm.my; hafiz@petroleum.utm.my

[1] Advanced Membrane Technology Research Centre (AMTEC), Faculty of Chemical and Energy Engineering, Universiti Teknologi Malaysia, N29a, 81310 Skudai, Johor, Malaysia

[2] Department of Materials, Faculty of Mechanical Engineering, Universiti Teknologi Malaysia, 81310 Skudai, Johor, Malaysia

[3] Department of Life Science and Applied Chemistry, Nagoya Institute of Technology, Gokiso-cho, Showa-ku, Nagoya 466-8555, Japan

[4] Nanotechnology Research Centre, Department of Physics, Faculty of Science and Mathematics, Universiti Pendidikan Sultan Idris, 35900 Tanjung Malim, Perak, Malaysia

[5] Department of Chemistry, Faculty of Science, Institut Teknologi Sepuluh Nopember, Kampus ITS Sukolilo, Surabaya 60111, Indonesia

Published online: 10 March 2020

Yamaguchi et al. [11] suggesting that the addition of AFL is able to act as a better contact layer. It can be observed through the improvement of both ohmic and polarization resistances by the addition of AFL. By taking advantages from the advancement in the SOFC, the AFL addition was required in to obtaining the optimized performance from the cell. With this reason, it can be concluded that the addition of AFL has functioned well as a bridge to reduce the contact resistance between anode and electrolyte.

The single-step fabrication of triple layer hollow fiber via phase inversion method was proven to be a method that can reduce time, cost, and chemical utilization as compared to the conventional method [16–18]. The method employed previously, such as ram extrusion, requires the cell to be sintered with each addition of component layer and thus used up more energy and time consuming [19–21]. With the phase inversion-based co-extrusion technique, all three layers can be sintered simultaneously, which can cut down the fabrication time [17, 22–24]. Follow up by sintering to remove the impurities and densify the hollow fiber. However, the simultaneous sintering of all three layers is challenging as all components having different shrinkage rate [25, 26]. Nevertheless, it can be overcome with the shrinkage analysis to measure optimal increment and time of sintering.

Hydrogen is a common fuel for SOFC. However, due to its low availability, there is still need to synthesis it [27]. Usually, hydrogen produced via several hydrocarbon reactions such as partial oxidation of methane [28], steam reforming [27], and dry reforming [29]. Due to the scarcity of the hydrogen, SOFC can be a complex system and thus increase its production costs. On the other hand, the issue of direct hydrocarbon as fuel for SOFC such as carbon poisoning still being debated until today [30].

SOFC fuel flexibility allows various sources of hydrocarbon to be applied such as methane [31], butane [32], and naphtha [33]. The anode of SOFC functioned as dual system by combining cracking and electro catalyst [34]. Therefore, when methane applied as fuel, there are few paths to be considered. The cracking of methane reaction requires anode to produce hydrogen and carbon before going through electrochemical reaction. The system still utilizes hydrogen as energy, but with different path of reaction. Instead of directly utilizing the hydrogen, the methane was cracked first. At a fuel-side triple point, the electrolyte (oxygen ion donor), the anode (electronic conductor), and the pore (source of the H_2 or CO molecule) meet. Oxygen ions (O^{2-}) are extracted from the electrolyte, and the following exothermic reactions occur:

$$\text{Reactions at anode}: H_2 + O^{2-} \rightarrow H_2O + 2e^-$$

$$CH_4 + 4O^{2-} \rightarrow CO_2 + 2H_2O + 8e^-$$

$$\text{Reaction at cathode}: \frac{1}{2}O_2 + 2e^- \rightarrow O^{2-}.$$

$$\text{SOFC overall reaction}: CH_4 + 2O_2 \rightarrow 2H_2O + CO_2$$

In this study, a triple layer hollow fiber consisting of anode/anode functional layer (AFL)/electrolyte was produced via co-extrusion/co-sintering method. After that the cathode deposition, the complete SOFC was undergone fuel cell performance test with methane as the fuel source. The fuel cell performance as a function of time was recorded to observe how TLHF could resist the carbon deposition phenomenon with methane as the fuel source.

Methodology

Materials

Ceramic materials used in this study were nickel oxide (NiO), yttria stabilized zirconia (YSZ), and lanthanum strontium manganite (LSM) from NexTech Materials Ltd. (Ohio, USA). Polyethersulfone (PESf) that was applied as the polymer binder was purchased from Radel A300, Ameco Performance, USA. *N*-Methylpyrrolidone (NMP) from Qrec was used as a solvent. Arlacel P135 (polyethylene glycol 30-dipolyhydroxystearate, Uniqema) was used as a dispersant.

Dope suspension preparation

Three ceramic suspensions of inner layer, AFL, and outer layer were prepared according to Table 1. All three layers were prepared by mixing ceramic powder, polymer binder, dispersant, and solvent in a ball mill machine (NQM-4, Yangzhuo, Nuoya Machinery Co.) [35]. The inner layer and AFL composing of nickel oxide (NiO) and yttria stabilize zirconia (YSZ) from fuel cell materials as the ceramic components, *N*-methyl pyrrolidone (NMP, Qrec) as solvent PESf (Aremco) as polymer binder, and Arlacel P135 as the dispersant. Meanwhile, the electrolyte suspension was made from YSZ, PESf, NMP, and Arlacel P135. The dope suspensions were ball milled for 48 h and degassed to remove air bubble.

The extrusion of anode/AFL/electrolyte was accurately done by using syringe pumps as referring to Li et al. [13]. All three suspensions were loaded in the syringe pumps.

Table 1 List of dope suspension and the composition

Materials	Anode (wt%)	AFL (wt%)	Electrolyte (wt%)
NiO	39	13	–
YSZ	26	52	60
NiO/YSZ ratio	6:4	2:8	–
NMP	28.38		33.88
PESf	6.5		6
Additive (Arlacel)	0.12		

After that, all the suspensions were simultaneously extruded into four orifice spinnerets by syringe pumps and free falling into the coagulation bath to form triple layer hollow fiber. The extrusion parameters were shown at Table 2. After the extrusion process completed, the membrane was collected and cut into 30 cm long per fiber and were straightened [36]. Following the 24-h drying, the precursor was ready to be sinter.

Sintering of the hollow fiber

Sintering process was done using tubular furnace (XY-1700, Nanyang Electric Equipment, China) with alumina insulator to reduce heat loss [37]. The co-sintering process started at room temperature and was increased by 2 °C/min until 400 °C and maintained for 1 h. Next, the temperature was increased again by 2 °C/min until it reached 800 °C and maintained for 1 h to remove impurities. After that, the temperature increased once more at rate of 2°/min until it reached 1500 °C and was maintained for 10 h. Finally, it allowed to cool down to room temperature at 5°/min.

Cathode deposition

The cathode deposition was done via brush painting method. The LSM was mixed with ethanol via stirring process. After that, the LSM was brushed on the surface of hollow fiber for 1 cm length. Next, it was dried at 60 °C for 10 min. Then, it was sintered at 900 °C for 5 h to ensure the cathode layer adhered to the hollow fiber.

Scanning electron microscopy

The sample was placed on the stub before the image could be captured. The sample was placed on a stub with double-sided tape. After that, the sample was coated with gold particle under vacuum condition. After undergone coating, the sample was captured by using SEM machine (Hitachi TM3030) with several magnifying.

Fuel cell performance test

The cell performance evaluation was carried out in a high temperature SOFC setup. The reactor was constructed by sealing each ends of the hollow fiber with alumina tubes by using ceramic sealant. Then, it was pre-fired at 240 °C for 3 h in order to make the sealant gas tight. The current collectors were placed inside the hollow and also at the cathode layer. In addition, platinum paste was applied on the cathode layer to minimize the voltage loss. The anode was exposed to 20 ml/min with methane while the cathode was exposed to oxygen. The current-voltage (I-V) curves and impedance were performed using potentio-galvanostat (Autolab) machine. The performance was measured between 700 and 800 °C for up to 90 min of operation.

Table 2 Extrusion condition and parameters

Air gap	10 cm
Flowrate of bore fluid	8 ml/min
Flowrate of anode	8 ml/min
Flowrate of AFL	2 ml/min
Flowrate of electrolyte	2 ml/min

Carbon analysis

Carbon weight analysis

After certain period of time, the cell went through carbon analysis. The sample operated for the periods of 30, 60, and 90 min was undergone carbon analysis by using LECO CS844. Firstly, the sample was grounded into powder. Then, 0.02 g of sample was placed in a crucible cup mixed with 1 g of iron chip accelerator (LECO). Finally, it was inserted into machine to be combusted 900 °C. The process repeated for other samples.

Transmission electron microscopy

The bulk hollow fibers were grinded using mortar and pestle into nanosized particles with diameter of approximately 20 nm. The nanoparticles were then directly mounted with other post treatment on the Cu mesh for TEM observation. The samples were observed under working pressure of 1×10^{-6} Pa using Atomic Resolution Analytical Microscope (JEOL ARM200F) with acceleration voltage 200 kV. The samples were observed at low magnification × 100,000 and high magnification × 500,000 to study the structural formation of Ni crystalline and graphitic layers.

Three-point bending test

The three-point bending test was used using Instron 3342 testing system. The sample was measured up to 6 cm due to the jig to put the sample around is 4.3 cm. The sample was placed on the center and should be located as close as possible to the load. After that, the load was dropped at the rate of 0.1 N per minute. Next, the maximum load was recorded and used in the Eq. 1 to obtain the mechanical strength.

$$B = \frac{8NLD_0}{\pi\left(D_0{}^4 - D_1{}^4\right)} \tag{1}$$

Where, N is maximum load of the sample, L is length of the sample, D_0 is outer diameter of the sample, and D_1 is inner layer of the sample.

Results and discussion

Characteristics of triple layer hollow fiber membrane

Figure 1 shows the morphology of the hollow fiber sintered at 1500 °C. The hollow fiber showed no delamination which indicated that all the layers had adhered to each other. The thickness of anode layer was 110 μm, AFL at 65 μm, and electrolyte at 58 μm. The anode layer shows the finger-like structure dominating the anode layer. This indicates there are actively solvent/non-solvent exchange during the co-extrusion process [38–40]. In addition, the long finger-like provides more reaction site hence producing higher power density. Meanwhile, there are also finger-like structure at AFL which is sandwiched between electrolyte and anode. In this regard, finger-like structure greatly mitigates the resistance of the gas flow from the center bore to the anode/electrolyte interface as the gas molecules preferentially flow through the micro-channels first and then access the interface by diffusion. The shorter finger like tends to have shorter conduction path that resulting more gas to diffuse in ionic form. As a result, the mass transport enhanced thus increasing the cell performances. This was proven by Dzarfan and co-workers [41–43] had found by altering the finger like of the anode, the power densities can be increased from the void thickness. The void thickness of 60% produces 2.03 Wcm^{-2} while the 70% void thickness resulting 2.32 Wcm^{-2}.

This is in contradiction with the finding reported by Li et al. [13] that shows AFL was a sponge-like structure. The structure of AFL in this study was produced via solvent/non-solvent exchange initiated by the adhesion process within the layer. Due to the deep phase inversion process that occurred at AFL, there are more finger-like formation was observed. There are also phase inversion occurred from the electrolyte layer. Due to the hydrophilic property of YSZ suspension [44], the penetration from the electrolyte layer produces the finger-like structure of AFL layer. Finally, the electrolyte layer showed dense layer was formed. The dense layer was crucial to prevent the fuel crossover. The dense layer also only allows oxygen to transport to the anode site in ionic form.

Stability study measurement

The open circuit voltage (OCV) was measured at different temperatures to determine the optimum temperature at which the methane actively underwent cracking reaction from CH_4 to C and H_2. Figure 2 shows the trend of OCV of hollow fiber with methane feed as a function of time. Based on the figure, it was observed that the initial OCV was at 1.1 V, which in agreement with the Nernst Equation. In addition, the high OCV at start shows the hollow fiber used was fully gas tight. Hence, there are no fuel crossover. As the operation prolonged, the OCV had decreased for all three operating temperatures (i.e., 700, 750, and 800 °C). At 700 °C, the degradation by far is the worst. The OCV recorded decreases from 1.1 V to 0.1 in the span of 90 min. Meanwhile, at 750 °C, the OCV recorded the decreases from 1.1 to 0.25 V in 90 min. Finally, when increase the operating temperature to 800 °C, the OCV recorded 1.1 V at 0 min and reduced to 0.99 V in 90 min. This was due to the carbon had been deposited on the triple phase boundary (TPB) area that leads to increase of the resistance and the electrolyte being cracked after prolonged operation. The increase of resistance by carbon is in agreement with the study done by Hanna et al. [45] which stated that the carbon formed deposited on the catalyst site, automatically poisoned the site that leads to less performance. Despite that, the temperature also plays role in the OCV. At higher

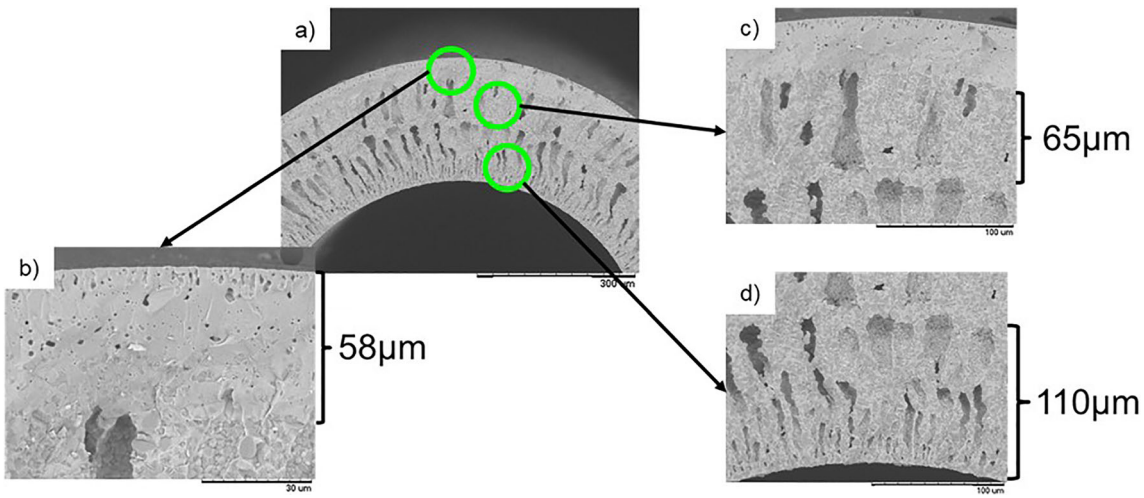

Fig. 1 SEM images of triple layer hollow fiber sintered at 1500 °C with **a** hollow fiber, **b** electrolyte layer, **c** AFL layer, and **d** anode layer

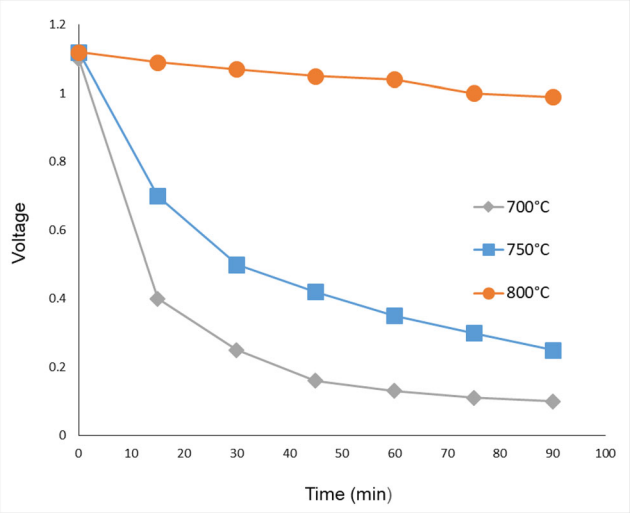

Fig. 2 OCV of cell with methane feed at different time and working temperature

temperature, the CH_4 cracking is more active. CH_4 being transformed into CO_2 are more active at higher temperature, producing less carbon deposit as the operation time increased. After the carbon deposits had been concentrated, the carbon penetrates throughout the AFL and electrolyte. The carbon produces void between the grain boundaries and allows more fuel crossover to occur.

In order to understand the voltage and power performance, the current-voltage (IV) curve was produced to determine the maximum power density. Figure 3 shows the power density at 800 °C under methane as fuel. The working temperature chosen at 800 °C due to the best performance was obtained at 800 °C. Figure 3 shows the power density was initially recorded at 0.8 Wcm^{-2}. The initial power density obtained was higher than mostly reported studies by using H_2 [46]. This can be explained by the hydrogen density in the methane was higher as compared to hydrogen. In addition, the

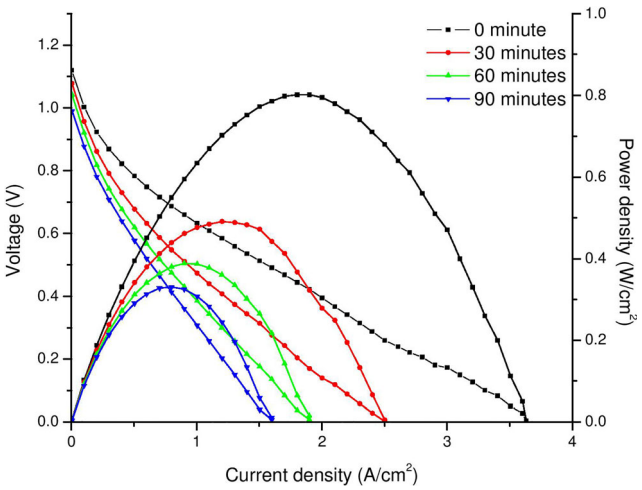

Fig. 3 I Performance test of hollow fiber at 800 °C at different operating time

hydrogen-rich environment produced by CH_4 has prolonged the H_2 gases to remain in the pore and TPB area. However, the anode suffers from stability issue from the usage of CH_4 as fuel. The maximum power density started to decrease as early as 30 min from 0.8 to 0.49 Wcm^{-2} and the trend continues afterwards. At 60 and 90 min, the power density recorded at 0.38 and 0.33 Wcm^{-2}, respectively. This is due to the carbon deposition had started to occur and led to the cell crack which consequently increase of fuel crossover. Further investigation on the cell structure will be discussed in the "Morphological changes after methane exposure" section. In addition, it also suggests that activation polarization caused the IV had such a highly curve. It also indicates that the anode pores had been filled with carbon-like molecule thus causes cell deactivation.

The trend can be correlated with the amount of carbon deposited onto the catalyst site in the anode. Initially, there are huge reaction site available. When the methane fuel was applied, the carbon had also started to deposit simultaneously via cracking of methane. At 30 min, the drastic decrement was observed. This indicates that there are many reaction site had been deposited with carbon. After that, at 60 min of operation time, the performance reduction has significantly decreased. This indicates that there is less reaction site to be deposited. Finally, at 90 min of operation, the carbon still caused performance reduction. However, since there are few reaction site available, the performance reduction was at its lowest. It also indicates that carbon deposition rate is lesser when the concentration increases.

Impedance analysis

Impedance analysis was performed to understand the polarization behavior of the cell. The impedance was done to show the effect of carbon deposition towards the resistance of the hollow fiber. Figure 4 shows the impedance analysis of hollow fiber after certain period of time. Impedance shows the resistance in the hollow fiber consisting of ohmic resistance and area specific resistance. Figure 4 shows ohmic resistance (OR) initially recorded at 0.13 Ωcm^2. The value was much higher mostly due to the electrolyte thickness that increases the resistance of the cell. After 30 min, the OR was increased to 0.27 Ωcm^2 indicating small number of carbon had been deposited. In other word, the peculiar fact is at temperature range of 500 to 800 °C, carbon that is in amorphous state nucleated around the Ni particles and spread until it covered the whole solid [47]. After 60 min, the OR increase to 0.38 Ωcm^2 indicating more carbon had been deposited and caused the fiber started to crack. Prolonged operation causes more carbon to be deposited in the anode region that causes activation to be more difficult for CH_4 cracking. The phenomenon of increasing resistance also contributed prolonged pathway for the electron transfer from the cathode to the anode.

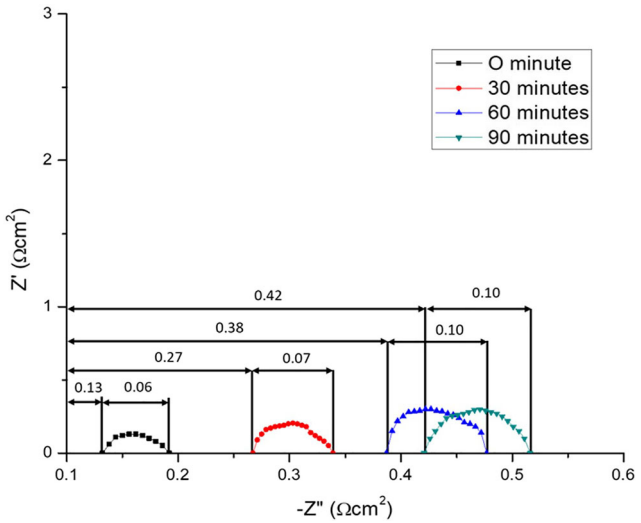

Fig. 4 Impedance analysis with methane fuel at 800 °C

Meanwhile, the area specific resistance (ASR) was started at 0.06 Ωcm^2. After 30 min, the ASR had increased to 0.07 Ωcm^2. Prolonged operation to 60 min increases the ASR until it reached 0.10 Ωcm^2. The ASR value shows the carbon deposits on the anode does reduce the performance via poisoning the anode surface. This phenomenon continues until the anode surface no longer underwent carbon cracking. At 60 onwards, the value of ASR did not change indicating the anode layer had been saturated with the carbon.

To understand how the carbon deposition affecting the performance, Fig. 5 demonstrates the mechanism of carbon deposits. Initially, the methane had been cracked to C and hydrogen gas. After that, the hydrogen reacts with the oxygen that had been reduced from the cathode. The carbon covers up the catalyst site on the anode. Even though there are reaction that converts carbon into CO and CO_2, the carbon easily deposited on Ni makes the conversion of the carbon gas are relatively very low as compared to the solid carbon. After minutes of operation, the carbon deposition affected the anode layer. The remaining catalyst site was still producing electricity; however, the power density had tremendously reduced courtesy of the carbon deposition. In this regard, coke formation on the surface of the anode has blocked the pore size of the anode and thus reduced the amount of fuel that reached to the anode site and eventually lead to the concentration polarization [48]. Cimenti and Hill also indicated that the gas composition at AFL was different than the bulk composition through catalytic deposition within conducting layer of the anode [49].

After the anode and AFL had been filled with carbon, the carbon still continuously deposited due to the carbon generated in the form of multilayer and crystalline. Usually, the ceramic had grain boundaries that connected between each particle. This grain boundary is the weakest point of the dense electrolyte layer. The carbon particles able to penetrate via grain boundaries that causing crack on the electrolyte. The phenomenon is briefly depicted in Fig. 6.

Morphological changes after methane exposure

After 90 min of operation, the hollow fiber was characterized via SEM. The purpose of SEM after the operation was to observe the carbon that had been deposited and caused the degradation on the anode structure. Figure 7 shows the SEM images of anode and surface of electrolyte after minutes of operation. SEM image shows that the carbon had been deposited as early as 30 min. It was observed via the increasing of the carbon deposited on the Ni-YSZ anode surface. Since there are small number of carbon deposited, it does not cause the crack at the grain boundaries of the electrolyte surface.

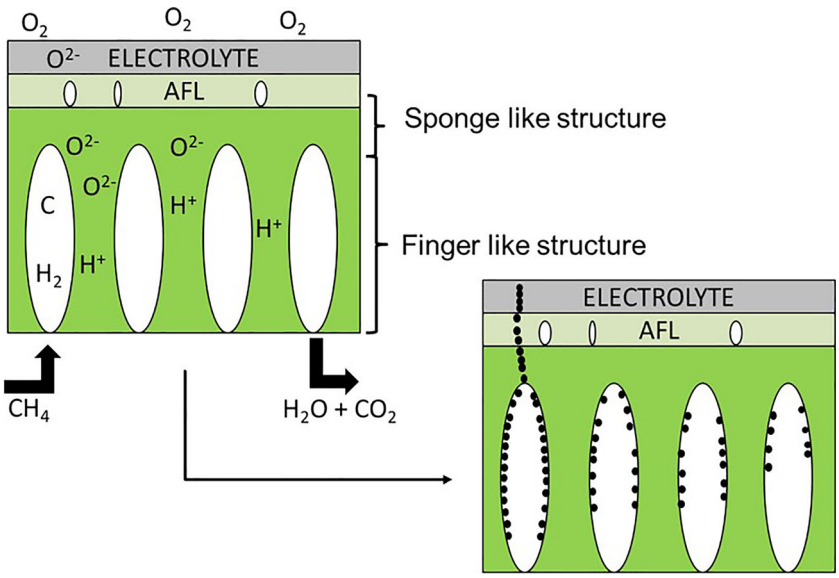

Fig. 5 Mechanism of carbon deposition

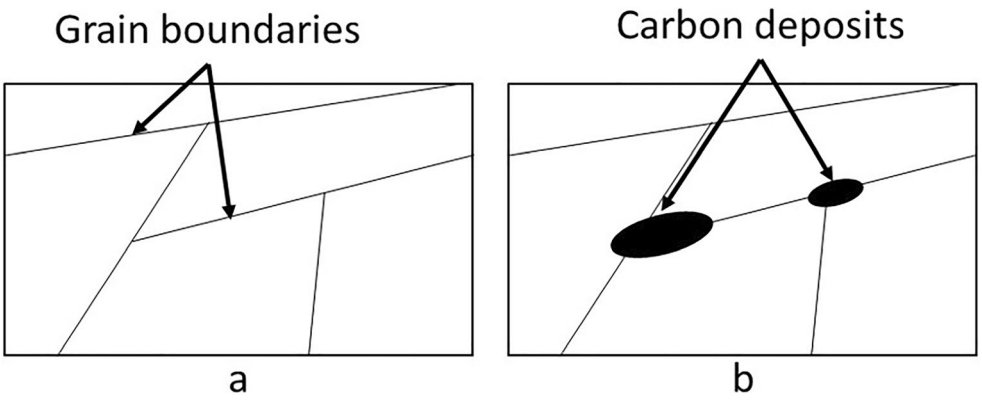

Fig. 6 Grain boundaries of electrolyte surface. **a** Before exposure. **b** After 90 min of operation

After 60 min of operation, the anode of hollow fiber was found to be promoting more carbon deposition. The carbon deposited increased due to the Ni had catalyzed more carbon with the increasing of exposing time. On the other hand, the grain boundaries of the electrolyte started to crack courtesy of the less densified area of electrolyte. It also explained the decrement of performance test where the OCV had dropped significantly. The crack on the electrolyte surface does promote fuel crossover, due to the existence of gas leakage in electrolyte.

After 90 min of operation, the Ni site has been deposited with carbon at which the carbon formed had creates poison-filled Ni structure. The crack can be obviously seen on the grain growth of the surface of electrolyte. Such crack causing the mechanical strength to decrease as proved by the 3-point bending strength results in Fig. 8, which show the decrease in mechanical strength of the hollow fiber from 135.3 to 63.2 MPa after 90 min. The carbon particle can be deposited in many forms from amorphous to graphitic. It was also related to the reaction rate of the methane itself. This was also related to the difference in reaction rate of CH_4 to CO_2. While there are many sets of reaction simultaneously in the hollow fiber, the hollow fiber does not only suffer on degradation in terms of performance, but in microstructure as well. The carbon did not only deposit, but also caused microstructural damage towards Ni. These findings had been confirmed

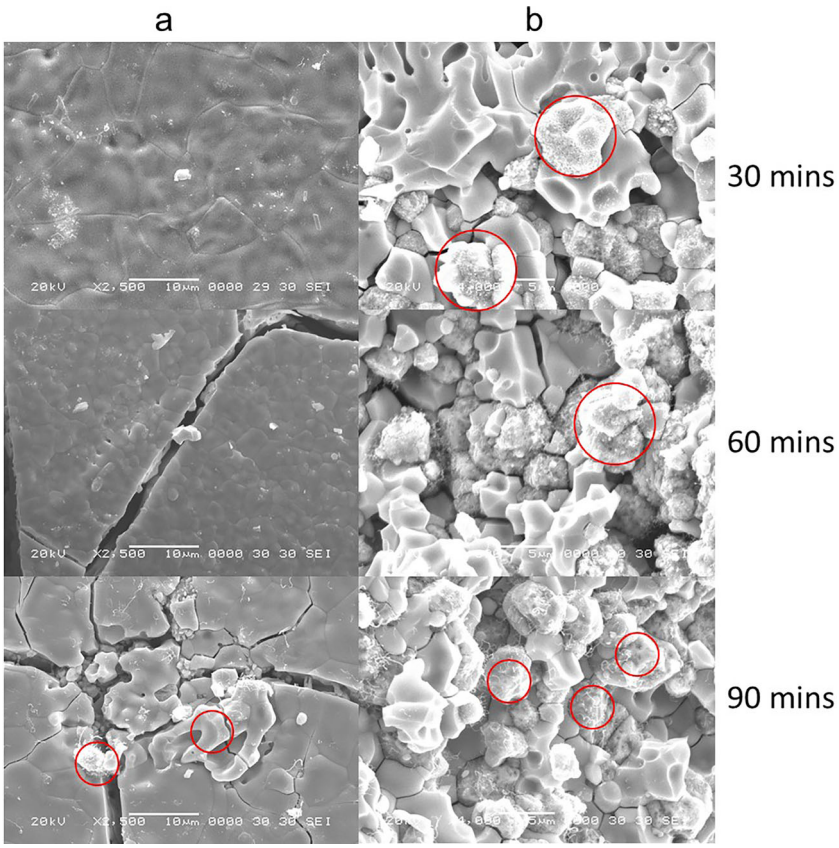

Fig. 7 SEM images of hollow fiber. **a** Outer surface of electrolyte. **b** Anode structures

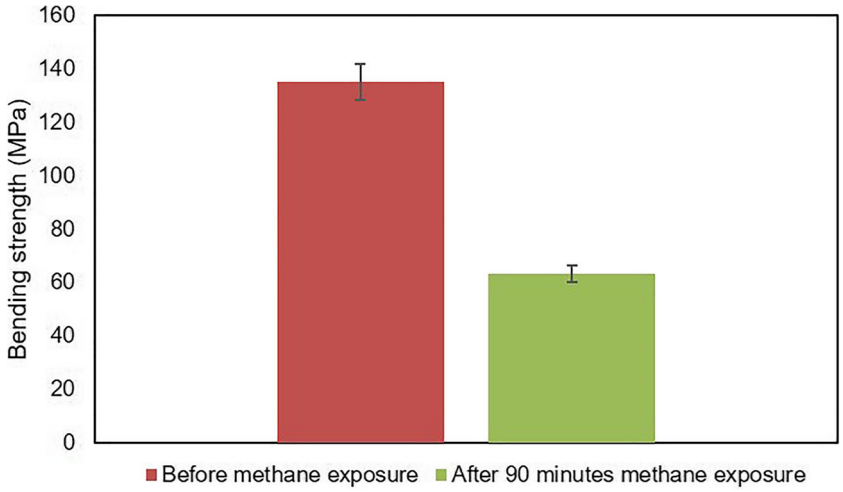

Fig. 8 Bending strength of triple layer hollow fiber with 80% YSZ content in AFL sintered at 1500 °C, before and after 90 min methane exposure

by He et al. [50]. The structural damage on the Ni was more severe at lower operating temperature. This contributed by the bulk dimension had been expanded. This also causing significant damage towards a working fuel cell due to the current had been interrupted for an extended period.

Figure 9 a to c show the TEM micrograph of hollow fiber with different carbon deposition time at 30 min, 60 min, and 90 min, respectively. The TEM analysis was done to observe the carbon formation on the surrounding of the nickel crystalline and the featured graphitic layers formation at high magnification. The carbon solubility of nickel is very high; hence, carbon atoms are easily diffuse in nickel crystal structure at high temperature (0.37% at 750 °C, [51]). Figure 9 a indicates that the carbon cloud were generally amorphous in nature as clearly observed at high magnification. High resolution TEM (HRTEM) showing small formation of crystal structure with lattice distance of 0.432 nm similar to nickel oxalate (C_2NiO_4) lattice distance (JCPDS 47-0798). The lack of deposition time (30 min) was believed to be restraining the carbon atoms bonding into graphitic formation hence leaving

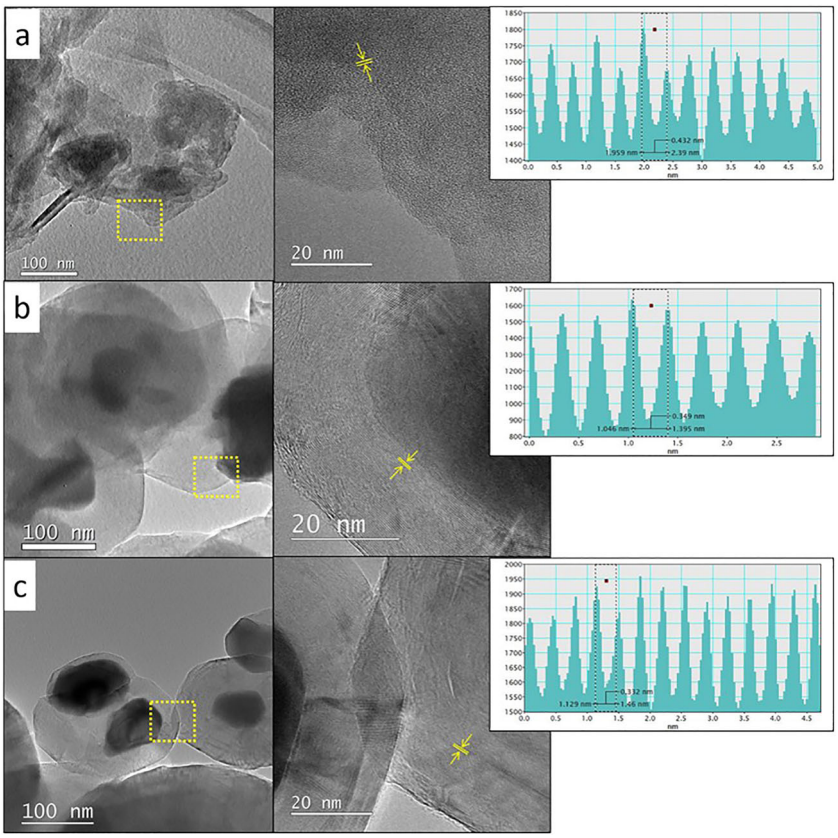

Fig. 9 TEM and HRTEM (inset) images of **a** 30, **b** 60, and **c** 90 min deposition time of carbon on nickel hollow fiber, respectively

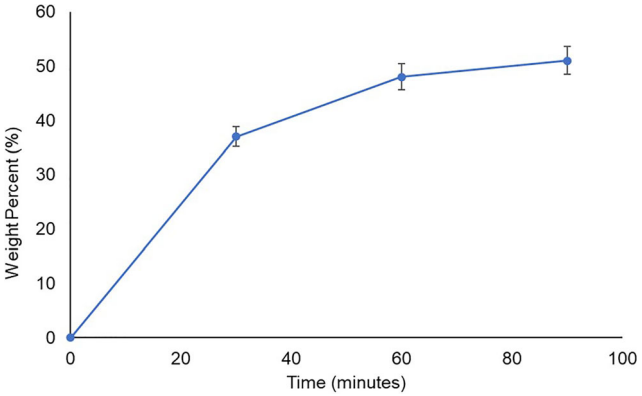

Fig. 10 Carbon content of hollow fiber operated at 800 °C at different time

only amorphous carbon structure shroud on the nickel particles. The TEM images for 60 min deposition time showed mixture formation of graphitic and amorphous carbon (Fig. 9b). The HRTEM (inset) shows thick graphitic layers formation (0.349 nm) surrounding nickel particles. The lattice distance of the layers matched the crystal lattice distance of graphite (JCPDS 75-0444). However, amorphous carbon was still observed in this sample indicating that 60 min of deposition and heating time were not sufficient.

Figure 9 c shows the 90 min deposition TEM images. Ninety minutes deposition time showed significant results of well graphitic layers formation surrounding the nickel particles. The HRTEM (inset) exhibited very thick graphitic layer formation (> 100 layers). HRTEM results also indicate that 90 min deposition time have thicker graphitic formation compared to 60 min deposition time which have around 70–80 graphitic layers. Figure 8 a–c confirming that the deposition and annealing time have great effect to the amorphous–graphitic formation of carbon atoms.

Figure 10 shows the carbon deposition at different time of operation. The carbon deposits mostly during the first 30 min. This is due to the fact that there are many active sites in the anode layer [52]. There are many TPB area for methane to be converted into carbon and hydrogen. Then, after the conversion takes place, the carbon that failed to convert into the carbon gases, instead of remaining as carbon material such as graphene or graphite [53] were reduced by LSM at cathode and transported via YSZ electrolyte due to the rate of methane cracking is higher than the rate of carbon reaction with O^{2-}. After 60 min, the carbon content increased by 8%, but not as much as the first 30 min. This showed that the carbon is filling the remaining active sites. These results are also in agreement with the IV curve result that the performance was reduced after 60 min but does not reduce as much as compared to the ones during the first 30 min. At 90 min of operation, the carbon deposition rates lowered, recording a slight increase. This shows that there are less TPB sites available for methane cracking.

Conclusion

Triple layer hollow fiber from NiO and YSZ had been successfully fabricated via co-extrusion technique. The co-sintering at 1500 °C exhibit good gas tightness and mechanical strength. The SEM images showed the anode layer and AFL consisting of finger-like structure forming sandwich-like structure. Meanwhile, the electrolyte layer formed dense structure which is required to prevent fuel crossover. The OCV initially recorded at 1.1 V and after a few minutes, the OCV decreases mostly at 700 °C and further lessen at 800 °C. The electrochemical test shows the maximum power density was recorded at 0.8 Wcm^{-2}. After 90 min of operation, the power density dropped to 0.3 Wcm^{-2}. The degradation was the worst in the first 15 min due to the abundance of reaction site. The impedance shows that the OR increased from 0.55 to 1.37 after 90 min indicating that the increase in conductivity was due to the carbon deposition. The SEM images showed that the carbon had been deposited and caused crack at the electrolyte layer. This phenomenon leads to the degradation in the cell performance due to the increase of the fuel crossover after 90 min. Meanwhile, the TEM images showed the progress of transforming from graphene into graphite on the anode layer. The methane fuel shows promising potential in SOFC operation, but the carbon deposition still remains as the biggest obstacle.

Acknowledgments The authors gratefully acknowledge financial support from Universiti Teknologi Malaysia under Research University Grant R&D Fund (Project number: Q.J130000.7746.4J309) and Tier 1 (Project number: Q.J130000.2546.16H40)). The authors would also like to thank Research Management Centre, Universiti Teknologi Malaysia for the technical support.

References

1. Li C-X, Li C-J, Guo L-J (2010) Effect of composition of NiO/YSZ anode on the polarization characteristics of SOFC fabricated by atmospheric plasma spraying. Int J Hydrog Energy 35(7):2964–2969
2. Howe KS, Thompson GJ, Kendall K (2011) Micro-tubular solid oxide fuel cells and stacks. J Power Sources 196(4):1677–1686
3. Zhao Y, Xia C, Jia L, Wang Z, Li H, Yu J, Li Y (2013) Recent progress on solid oxide fuel cell: lowering temperature and utilizing non-hydrogen fuels. Int J Hydrog Energy 38(36):16498–16517
4. Kendall K, Minh NQ, Singhal SC (2003) *Chapter 8—cell and stack designs*, in *high temperature and solid oxide fuel cells*. Elsevier Science, Amsterdam, pp 197–228
5. Akhtar N, Kendall K (2011) Micro-tubular, solid oxide fuel cell stack operated under single-chamber conditions. Int J Hydrog Energy 36(20):13083–13088
6. Meng X, Yang N, Meng B, Tan X, Yin Y, Ma Z-F, Sunarso J (2012) Microstructure tailoring of the nickel–yttria stabilised zirconia (Ni–YSZ) cermet hollow fibres. Ceram Int 38(8):6327–6334
7. Hatchwell C, Sammes NM, Brown IWM, Kendall K (1999) Current collectors for a novel tubular design of solid oxide fuel cell. J Power Sources 77(1):64–68

8. Grande FD, Thursfield A, Kanawka K, Droushiotis N, Doraswami U, Li K, Kelsall G, Metcalfe IS (2009) Microstructure and performance of novel Ni anode for hollow fibre solid oxide fuel cells. Solid State Ionics 180(11–13):800–804
9. Bi L, Fabbri E, Traversa E (2012) Effect of anode functional layer on the performance of proton-conducting solid oxide fuel cells (SOFCs). Electrochem Commun 16(1):37–40
10. Zhang X, Qiu YE, Jin F, Guo F, Song Y, Zhu B (2013) *A highly active anode functional layer for solid oxide fuel cells based on proton-conducting electrolyte BaZr0.1Ce0.7Y0.2O3−δ*. J Power Sources 241:654–659
11. Yamaguchi T, Sumi H, Hamamoto K, Suzuki T, Fujishiro Y, Carter JD, Barnett SA (2014) Effect of nanostructured anode functional layer thickness on the solid-oxide fuel cell performance in the intermediate temperature. Int J Hydrog Energy 39(34):19731–19736
12. Meng X, Yang N, Gong X, Yin Y, Ma Z-F, Tan X, Shao Z, Liu S (2015) Novel cathode-supported hollow fibers for light weight micro-tubular solid oxide fuel cells with an active cathode functional layer. J Mater Chem A 3(3):1017–1022
13. Li T, Wu Z, Li K (2015) Co-extrusion of electrolyte/anode functional layer/anode triple-layer ceramic hollow fibres for micro-tubular solid oxide fuel cells–electrochemical performance study. J Power Sources 273:999–1005
14. Suzuki T, Sugihara S, Yamaguchi T, Sumi H, Hamamoto K, Fujishiro Y (2011) Effect of anode functional layer on energy efficiency of solid oxide fuel cells. Electrochem Commun 13(9):959–962
15. Chen K, Chen X, Lü Z, Ai N, Huang X, Su W (2008) Performance of an anode-supported SOFC with anode functional layers. Electrochim Acta 53(27):7825–7830
16. Mohd Hafiz Dzarfan O, Mukhlis AR, Kang L, Juhana J, Hasrinah H, Ahmad Fauzi I (2015) *Ceramic hollow-fiber support through a phase inversion-based extrusion/sintering technique for high-temperature energy conversion systems*, in *Membrane Fabrication*. CRC Press, Boca Raton, pp 347–382
17. Mohd Hafiz Dzarfan Othman, Siti Munira Jamil, Mukhlis A. Rahman, Juhana Jaafar and A.F. Ismail, *Electrolyte hollow fiber as support via phase-inversion-based extrusion/sintering technique for micro tubular solid oxide fuel cell*, in *Frontiers in Ceramic Science*. 2017. p. 107–131
18. Wang H, Liu J (2012) Effect of anode structure on performance of cone-shaped solid oxide fuel cells fabricated by phase inversion. Int J Hydrog Energy 37(5):4339–4345
19. Mahmud LS, Muchtar A, Somalu MR (2017) Challenges in fabricating planar solid oxide fuel cells: a review. Renew Sust Energ Rev 72:105–116
20. He B, Ling Y, Xu J, Zhao L, Cheng J (2014) Effect of nickel impregnated hollow fiber anode for micro tubular solid oxide fuel cells. J Power Sources 258:391–394
21. Meng X, Gong X, Yin Y, Yang N, Tan X, Ma Z-F (2014) Effect of the co-spun anode functional layer on the performance of the direct-methane microtubular solid oxide fuel cells. J Power Sources 247: 587–593
22. Li T, Wu Z, Li K (2014) Single-step fabrication and characterisations of triple-layer ceramic hollow fibres for micro-tubular solid oxide fuel cells (SOFCs). J Membr Sci 449:1–8
23. Sun W, Zhang N, Mao Y, Sun K (2012) Fabrication of anode-supported Sc2O3-stabilized-ZrO2 electrolyte micro-tubular solid oxide fuel cell by phase-inversion and dip-coating. Electrochem Commun 20:117–120
24. Meng X, Yan W, Yang N, Tan X, Liu S (2015) Highly stable microtubular solid oxide fuel cells based on integrated electrolyte/anode hollow fibers. J Power Sources 275:362–369
25. Droushiotis N, Othman MHD, Doraswami U, Wu Z, Kelsall G, Li K (2009) Novel co-extruded electrolyte–anode hollow fibres for solid oxide fuel cells. Electrochem Commun 11(9):1799–1802
26. Park SY, Ahn JH, Jeong CW, Na CW, Song RH, Lee JH (2014) Ni-YSZ-supported tubular solid oxide fuel cells with GDC interlayer between YSZ electrolyte and LSCF cathode. Int J Hydrog Energy 39(24):12894–12903
27. Balachandran U, Dusek JT, Maiya PS, Ma B, Mieville RL, Kleefisch MS, Udovich CA (1997) Ceramic membrane reactor for converting methane to syngas. Catal Today 36(3):265–272
28. Asano K, Hibino T, Iwahara H (1995) A novel solid oxide fuel-cell system using the partial oxidation of methane. J Electrochem Soc 142(10):3241–3245
29. Assabumrungrat S, Laosiripojana N, Piroonlerkgul P (2006) Determination of the boundary of carbon formation for dry reforming of methane in a solid oxide fuel cell. J Power Sources 159(2):1274–1282
30. Lee D, Myung J, Tan J, Hyun S-H, Irvine JTS, Kim J, Moon J (2017) Direct methane solid oxide fuel cells based on catalytic partial oxidation enabling complete coking tolerance of Ni-based anodes. J Power Sources 345:30–40
31. Zhu H, Wang W, Ran R, Shao Z (2013) A new nickel–ceria composite for direct-methane solid oxide fuel cells. Int J Hydrog Energy 38(9):3741–3749
32. Wang Y-G, Sun L-L, Luo L-H, Wu Y-F, Liu L-L, Shi J-J (2014) The study of portable direct-flame solid oxide fuel cell (DF-SOFC) stack with butane fuel. J Fuel Chem Technol 42(9):1135–1139
33. Kim T, Liu G, Boaro M, Lee SI, Vohs JM, Gorte RJ, Al-Madhi OH, Dabbousi BO (2006) A study of carbon formation and prevention in hydrocarbon-fueled SOFC. J Power Sources 155(2):231–238
34. da Silva CA, de Miranda PEV (2015) Synthesis of LaAlO3 based materials for potential use as methane-fueled solid oxide fuel cell anodes. Int J Hydrog Energy 40(32):10002–10015
35. Harun Z, Hubadillah SK, Hasan S, Yunos MZ (2014) *Effect of thermodynamic properties on porosity of ceramic membrane prepared by phase inversion*. Appl Mech Mater 575:31–35
36. Hubadillah SK, Othman MHD, Ismail AF, Rahman MA, Jaafar J, Iwamoto Y, Honda S, Dzahir MIHM, Yusop MZM (2018) Fabrication of low cost, green silica based ceramic hollow fibre membrane prepared from waste rice husk for water filtration application. Ceram Int 44(9):10498–10509
37. Hubadillah SK, Othman MHD, Ismail AF, Rahman MA, Jaafar J (2018) A low cost hydrophobic kaolin hollow fiber membrane (h-KHFM) for arsenic removal from aqueous solution via direct contact membrane distillation. Sep Purif Technol
38. Hubadillah SK, Othman MHD, Matsuura T, Rahman MA, Jaafar J, Ismail AF, Amin SZM (2018) Green silica-based ceramic hollow fiber membrane for seawater desalination via direct contact membrane distillation. Sep Purif Technol 205:22–31
39. Kingsbury BFK, Li K (2009) A morphological study of ceramic hollow fibre membranes. J Membr Sci 328(1–2):134–140
40. Wang B, Lai Z (2012) Finger-like voids induced by viscous fingering during phase inversion of alumina/PES/NMP suspensions. J Membr Sci 405–406:275–283
41. Othman MHD, Droushiotis N, Wu Z, Kelsall G, Li K (2012) Dual-layer hollow fibres with different anode structures for micro-tubular solid oxide fuel cells. J Power Sources 205:272–280
42. Othman, M.H.D., Droushiotis, N., Wu, Z., Kelsall, G., and Li, K., High-performance, anode-supported, microtubular SOFC prepared from single-step-fabricated, dual-layer hollow fibers. Advanced Materials, 2011. 23(21): p. 2480–2483
43. Othman MHD, Wu Z, Droushiotis N, Kelsall G, Li K (2010) Morphological studies of macrostructure of Ni–CGO anode hollow fibres for intermediate temperature solid oxide fuel cells. J Membr Sci 360(1–2):410–417
44. Bayati R, Molaei R, Richmond A, Nori S, Wu F, Kumar D, Narayan J, Reynolds JG, Reynolds CL (2014) Modification of properties of yttria stabilized zirconia epitaxial thin films by excimer laser annealing. ACS Appl Mater Interfaces 6(24):22316–22325

45. Hanna J, Lee WY, Shi Y, Ghoniem AF (2014) Fundamentals of electro- and thermochemistry in the anode of solid-oxide fuel cells with hydrocarbon and syngas fuels. Prog Energy Combust Sci 40: 74–111
46. Chen K, Lü Z, Ai N, Huang X, Zhang Y, Ge X, Xin X, Chen X, Su W (2007) Fabrication and performance of anode-supported YSZ films by slurry spin coating. Solid State Ionics 177(39–40):3455–3460
47. Baker RTK, Barber MA, Harris PS, Feates FS, Waite RJ (1972) Nucleation and growth of carbon deposits from the nickel catalyzed decomposition of acetylene. J Catal 26(1):51–62
48. Trimm DL (1997) Coke formation and minimisation during steam reforming reactions. Catal Today 37(3):233–238
49. Cimenti M, Hill MJ (2009) *Direct utilization of liquid fuels in SOFC for portable applications: challenges for the selection of alternative anodes*. Energies 2(2)
50. He H, Hill JM (2007) Carbon deposition on Ni/YSZ composites exposed to humidified methane. Appl Catal A Gen 317(2):284–292
51. Yang RT, Goethel PJ, Schwartz JM, Lund CRF (1990) Solubility and diffusivity of carbon in metals. J Catal 122(1):206–210
52. Sumi H, Lee Y-H, Muroyama H, Matsui T, Kamijo M, Mimuro S, Yamanaka M, Nakajima Y, Eguchi K (2011) Effect of carbon deposition by carbon monoxide disproportionation on electrochemical characteristics at low temperature operation for solid oxide fuel cells. J Power Sources 196(10):4451–4457
53. Sameshima S, Furukawa N, Hirata Y, Shimonosono T (2014) Cell performance of SOFC using CH4–CO2 mixed gases. Ceram Int 40(4):6279–6284